

ELASTIC BUCKLING OF A RECTANGULAR SANDWICH PLATE WITH AN INDIVIDUAL FUNCTIONALLY GRADED CORE

KRZYSZTOF MAGNUCKI

Lukasiewicz Research Network – Poznan Institute of Technology, Poznan, Poland

EWA MAGNUCKA-BLANDZI

Poznan University of Technology, Institute of Mathematics, Poznan, Poland

KRZYSZTOF SOWIŃSKI

Poznan University of Technology, Institute of Applied Mechanics, Poznan, Poland

e-mail: krzysztof.sowinski@put.poznan.pl

This paper is devoted to a thin-walled sandwich plate with an individual functionally graded core. The nonlinear shear deformation theory of a straight normal line is applied. A system of three differential equations of equilibrium of this plate is obtained, based on the principle of stationary potential energy, which is reduced to two differential equations and solved analytically. The critical load of the rectangular sandwich plate is determined. A detailed analytical study is carried out for selected exemplary plates. Moreover, a numerical FEM model of this plate is developed. The results of these calculations are compared with each other.

Keywords: buckling, sandwich structures, shear deformation theory, functionally graded core

1. Introduction

Composite materials have attracted considerable interest in recent decades. Their properties, including a high strength-to-mass ratio and exceptional stiffness providing significant buckling resistance, allow designing of more effective structures. Unlike homogeneous materials, they are characterised by variable properties toward one or more specific directions, which, to some extent, can be controlled by manufacturing processes. It gives an opportunity to control their mechanical behaviour such as deformation or the dynamic response. These advantages make them highly desired structures in numerous branches of the industry, including the aerospace industry, biomedical engineering, civil and marine engineering.

The application of composites, including thin-walled sandwich structures and functionally graded materials (FGMs), requires appropriate tools to study and predict their behaviour. As classical beam, plate, and shell theories cannot capture their variable properties, it is necessary to formulate new theories and assess their accuracy. This topic gained significant attention; thus, many researchers are striving to provide more unified and general analytical formulations. In the last two decades, a significant advancement has been achieved in this field.

Yang and Qiao (2005) developed a higher-order impact model aiming to simulate the free-vibration response of a soft-core sandwich beam subjected to a foreign object impact. Carrera and Brischetto (2009) described a large variety of plate theories including higher-order, zig-zag, layerwise, and mixed theories to evaluate bending and vibration of sandwich structures. By performing an asymptotic analysis of three-dimensional linear elasticity, Berdichevsky (2010) developed a two-dimensional theory of sandwich plates. Bouazza *et al.* (2010) presented a numerical study on bending of symmetrically laminated plates, where attention was paid to the shear effect.

Meiche *et al.* (2011) proposed an enhanced theory of hyperbolic shear deformation that takes into account transverse shear deformation effects and may be used to analyse free vibration problems in thick, functionally graded sandwich panels. Mantari *et al.* (2012) proposed an innovative shear deformation theory for sandwich and composite plates that parameterized the displacement field. The authors demonstrated that their theory and three-dimensional elasticity-bending solutions were in good agreement.

Grover *et al.* (2013) presented a new inverse hyperbolic shear deformation theory and validated it for a variety of numerical examples of laminated composite and sandwich plates considering static and buckling responses. Lopatin and Morozov (2013) focused on solving the buckling problem of a uniformly compressed rectangular composite sandwich plate with varying boundary conditions. The authors referred to the Lagrange principle and the first-order shear deformation theory to formulate the variational buckling equation.

For the static analysis of laminated composite and sandwich panels, Sahoo and Singh (2014) introduced a novel inverse trigonometric zigzag theory that was elaborated in their paper. The theory assumed a higher-order displacement field that satisfied the continuity requirements at the layer interfaces across the thickness of the plate. Kołakowski and Mania (2015) investigated the dynamic interactive response of square FGM plates subjected to an in-plane pulse loading using the modified classical laminate plate theory. Marczak and Jędrzyśiak (2015) studied free vibration of periodic three-layered sandwich structures referring to the Kirchhoff thin plate theory and the tolerance averaging technique. Sobhy (2016) introduced a novel shear deformation plate theory to study hygrothermal vibration and buckling of FGM sandwich plates supported by an elastic foundation.

Bouazza and Benseddiq (2015) focused on analytical modelling of thermoelastic buckling behaviour of functionally graded rectangular plates using a hyperbolic shear deformation theory. Ellali *et al.* (2015) derived an exact analytical solution for mechanical buckling analysis of a magnetoelectroelastic plate resting on the Pasternak foundation referring to the third-order shear deformation plate theory. The use of sandwich structures and the current state of mathematical modelling were explored by Birman and Kardomateas (2018). The authors focused on various core types, development of nanotubes, intelligent materials, and functionally graded properties of sandwich structures.

Magnucki *et al.* (2019) studied buckling and vibration of a rectangular plate with symmetrically variable mechanical properties across its thickness. The proposed nonlinear deformation hypothesis was assumed, while the derivation was based on the Hamilton principle. Bouazza *et al.* (2019) investigated bending behaviour of laminated composite plates. They studied a multilayer plate by the shear deformation theory and finite element method. Adhikari *et al.* (2020) focused on modelling the effect of porosity-type defects and analysing their effect on buckling behaviour of various types of FGM sandwich combinations, including multiple arrangements of layers. Foroutan *et al.* (2021) developed a unified formulation of a fully geometrically nonlinear refined plate theory in a total Lagrangian approach. The study aimed to analyse the post-buckling and large deflection behaviour of a sandwich FGM plate with a porous core. Magnucka-Blandzi *et al.* (2021) studied bending and buckling problems for simply supported circular plates with mechanical properties that varied symmetrically in the thickness direction.

Magnucki and Magnucka-Blandzi (2021) devoted their work to generalisation of the analytical model of sandwich structures. A continuous variation of mechanical properties across the thickness was assumed, whereas the problem was formulated referring to the principle of stationary potential energy.

Aguib *et al.* (2021) studied buckling of a plate made of steel and a magnetorheological elastomer subject to a compressive load. Analytical models of sandwich beams, homogeneous beams with bisymmetric cross sections, and beams with symmetrically variable mechanical characteristics were presented by Magnucki (2022). They were developed utilising a novel shear deformation

theory that was inspired by the Zhuravsky shear stress formula. Katili *et al.* (2023) described the problem of buckling of FGM sandwich plates in the numerical FEM analysis. Magnucki *et al.* (2023) using the generalised theory of deformation studied the buckling problem of an axially compressed generalised cylindrical sandwich panel and a rectangular sandwich plate.

Many studies in the field of composite structures investigate the problem of buckling using a specific shear deformation theory, where the form of shear deformation function is assumed in advance, e.g. trigonometric, inverse trigonometric, hyperbolic, or inverse hyperbolic. In the presented paper, the buckling of a simply supported rectangular thin-walled plate of length a , width b , and total thickness h is resolved using the nonlinear shear deformation theory, where the shear deformation function is obtained analytically with consideration of the classical shear stress formula. In contrast to other shear deformation theories, in the presented formulation, the accuracy of the solution does not depend on the pre-defined shear deformation functions. Instead of predicting these functions here, the classical shear stress formula recalled by Magnucki (2022) is applied to analytically solve the shear deformation function. Moreover, the proposed formulation enables studying the composite structures with variable mechanical properties described by complex functions.

The plate is compressed in the middle plane with a uniformly distributed load of the intensities N_x and N_y (Fig. 1). Young's modulus of the core is assumed to be described by a parametric function that allows one to describe homogeneous, three-layer, and five-layer structures. This approach constitutes a generalisation of sandwich structures, which is possible by introducing an individual functionally graded core. The stiffness ratio between yjr layers can be optional, whereas transition of Young's modulus between them is smooth. The main objective of this paper is to develop analytical and numerical models and the determine the critical load of the plates.

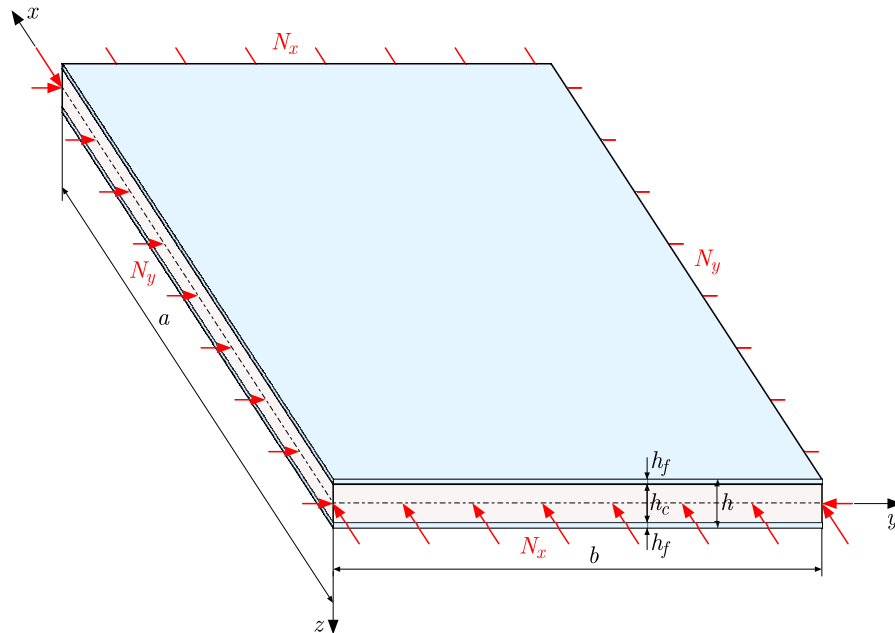


Fig. 1. Scheme of the rectangular sandwich plate compressed in the middle plane

The total thickness of the plate is the sum of the following layers

$$h = 2h_f + h_c \quad (1.1)$$

where: h_f – thicknesses of the faces, h_c – thickness of the core.

2. Analytical model of the rectangular sandwich plate

Young's modulus varies in the direction of thickness of the plate as follows:

— the upper face ($-1/2 \leq \zeta \leq -\chi_c/2$) and the lower face ($\chi_c/2 \leq \zeta \leq 1/2$)

$$E_f(\zeta) = E_f = \text{const} \quad (2.1)$$

— the core ($-\chi_c/2 \leq \zeta \leq \chi_c/2$)

$$E_c(\zeta) = E_f f_c(\zeta) \quad (2.2)$$

where the dimensionless function is

$$f_c(\zeta) = e_c + (1 - e_c) \left[\frac{1}{2} + \frac{1}{2} \cos\left(4\pi \frac{\zeta}{\chi_c}\right) \right]^{n_e} - k \left[\cos\left(\pi \frac{\zeta}{\chi_c}\right) \right]^{10n_e} \quad (2.3)$$

and $\zeta = z/h$ denotes the dimensionless coordinate, $\chi_c = h_c/h$ – relative thickness of the core, e_c – coefficient of Young's modulus ($0 < e_c \ll 1$), n_e – exponent-natural number, k – coefficient ($0 \leq k \leq 1 - e_c$). An exemplary variation of Young's modulus in the direction of plate thickness is shown graphically in Fig. 2, assuming $e_c = 0.2$, $k = 0.1$, $n = 7$.

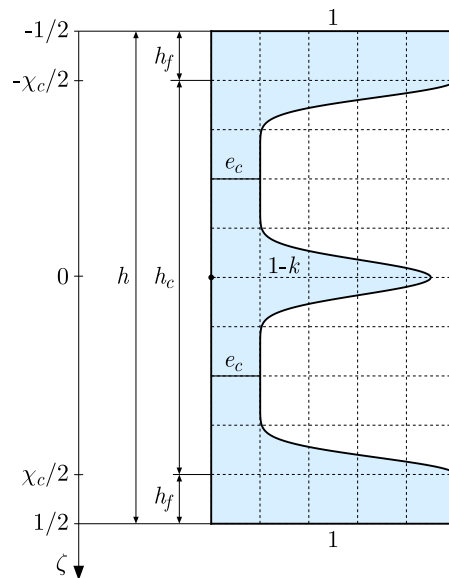


Fig. 2. Variation of Young's modulus in the direction of plate thickness

The deformation of the straight normal line to the neutral surface after buckling of this rectangular plate is shown in Fig. 3.

The longitudinal displacements according to Fig. 3 are as follows:

— the upper face ($-1/2 \leq \zeta \leq -\chi_c/2$)

$$u^{(uf)}(x, y, \zeta) = -h \left[\zeta \frac{\partial w}{\partial x} - f_d^{(uf)}(\zeta) \psi_f(x, y) \right] \quad (2.4)$$

$$v^{(uf)}(x, y, \zeta) = -h \left[\zeta \frac{\partial w}{\partial y} - f_d^{(uf)}(\zeta) \varphi_f(x, y) \right]$$

— the core ($-\chi_c/2 \leq \zeta \leq \chi_c/2$)

$$u^{(c)}(x, y, \zeta) = -h \left[\zeta \frac{\partial w}{\partial x} - f_d^{(c)}(\zeta) \psi_f(x, y) \right] \quad (2.5)$$

$$v^{(c)}(x, y, \zeta) = -h \left[\zeta \frac{\partial w}{\partial y} - f_d^{(c)}(\zeta) \varphi_f(x, y) \right]$$

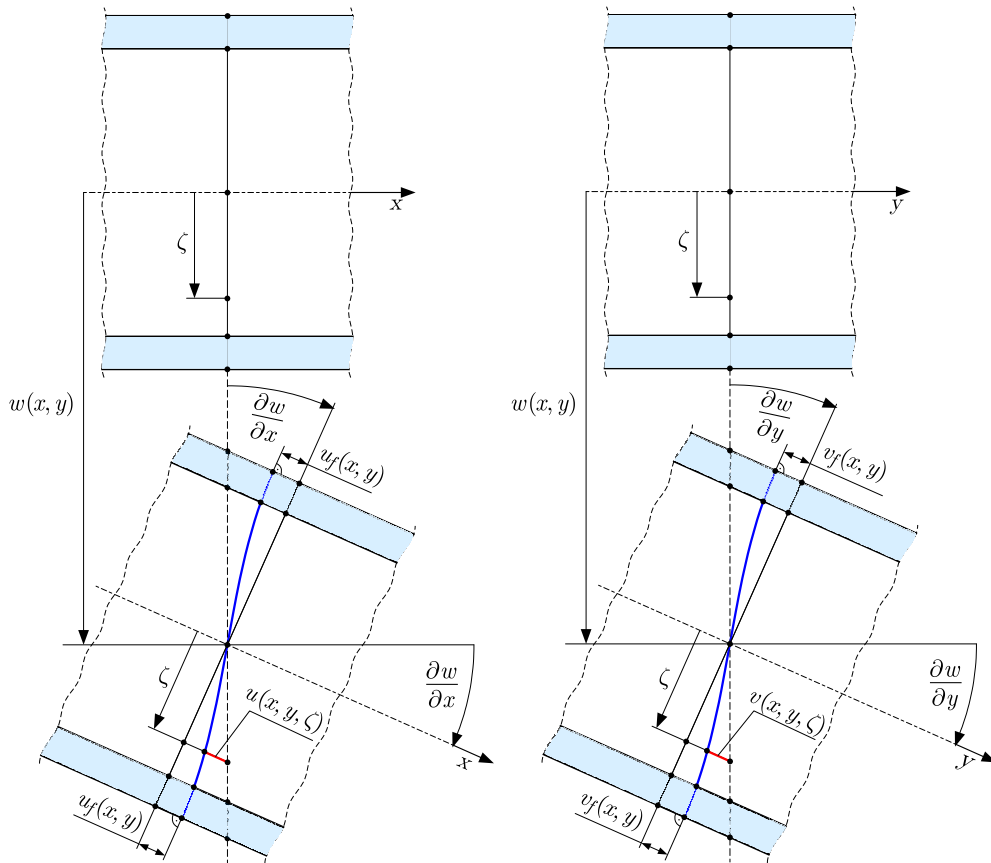


Fig. 3. The deformation scheme of the straight normal line of the plate

— the lower face ($\chi_c/2 \leq \zeta \leq 1/2$)

$$\begin{aligned} u^{(lf)}(x, y, \zeta) &= -h \left[\zeta \frac{\partial w}{\partial x} - f_d^{(lf)}(\zeta) \psi_f(x, y) \right] \\ v^{(lf)}(x, y, \zeta) &= -h \left[\zeta \frac{\partial w}{\partial y} - f_d^{(lf)}(\zeta) \varphi_f(x, y) \right] \end{aligned} \quad (2.6)$$

where: $w(x, y)$ – deflection, $\psi_f(x, y) = u_f(x, y)/h$ and $\varphi_f(x, y) = v_f(x, y)/h$ – dimensionless displacement functions of the faces. Moreover, taking into account the papers by Magnucki (2022) and Magnucki *et al.* (2023), the dimensionless deformation functions of the straight normal line in the successive layers are of the form

$$\begin{aligned} f_d^{(uf)}(\zeta) &= -C_f + \frac{1}{24}(3 - 4\zeta^2)\zeta & f_d^{(c)}(\zeta) &= \int \frac{\overline{Q}_z^{(c)}(\zeta)}{f_c(\zeta)} d\zeta \\ f_d^{(lf)}(\zeta) &= C_f + \frac{1}{24}(3 - 4\zeta^2)\zeta \end{aligned} \quad (2.7)$$

where

$$\begin{aligned} \overline{Q}_z^{(c)}(\zeta) &= \frac{1}{8} [1 - \chi_c^2 + e_c(\chi_c^2 - 4\zeta^2)] - (1 - e_c)J_1(\zeta) + kJ_2(\zeta) \\ J_1(\zeta) &= \int_{-\chi_c/2}^{\zeta} \left[\frac{1}{2} + \frac{1}{2} \cos\left(4\frac{\pi}{\chi_c}\zeta_1\right) \right]^{n_e} \zeta_1 d\zeta_1 \end{aligned}$$

$$J_2(\zeta) = \int_{-\chi_c/2}^{\zeta} \left[\cos\left(\frac{\pi}{\chi_c} \zeta_1\right) \right]^{10n_e} \zeta_1 d\zeta_1$$

$$C_f = -\frac{1}{48}(3 - \chi_c^2)\chi_c + \int_0^{\chi_c/2} \frac{Q_z^{(c)}(\zeta)}{f_c(\zeta)} d\zeta$$

Thus, the strains can be described in the following manner.

— the upper face ($-1/2 \leq \zeta \leq -\chi_c/2$)

$$\begin{aligned} \varepsilon_x^{(uf)}(x, y, \zeta) &= -h \left[\zeta \frac{\partial^2 w}{\partial x^2} - f_d^{(uf)}(\zeta) \frac{\partial \psi_f}{\partial x} \right] \\ \varepsilon_y^{(uf)}(x, y, \zeta) &= -h \left[\zeta \frac{\partial^2 w}{\partial y^2} - f_d^{(uf)}(\zeta) \frac{\partial \varphi_f}{\partial y} \right] \\ \gamma_{xy}^{(uf)}(x, y, \zeta) &= -h \left[2\zeta \frac{\partial^2 w}{\partial x \partial y} - f_d^{(uf)}(\zeta) \left(\frac{\partial \psi_f}{\partial y} + \frac{\partial \varphi_f}{\partial x} \right) \right] \\ \gamma_{xz}^{(uf)}(x, y, \zeta) &= \frac{df_d^{(uf)}}{d\zeta} \psi_f(x, y) \quad \gamma_{yz}^{(uf)}(x, y, \zeta) = \frac{df_d^{(uf)}}{d\zeta} \varphi_f(x, y) \end{aligned} \quad (2.8)$$

— the core ($-\chi_c/2 \leq \zeta \leq \chi_c/2$)

$$\begin{aligned} \varepsilon_x^{(c)}(x, y, \zeta) &= -h \left[\zeta \frac{\partial^2 w}{\partial x^2} - f_d^{(c)}(\zeta) \frac{\partial \psi_f}{\partial x} \right] \quad \varepsilon_y^{(c)}(x, y, \zeta) = -h \left[\zeta \frac{\partial^2 w}{\partial y^2} - f_d^{(c)}(\zeta) \frac{\partial \varphi_f}{\partial y} \right] \\ \gamma_{xy}^{(c)}(x, y, \zeta) &= -h \left[2\zeta \frac{\partial^2 w}{\partial x \partial y} - f_d^{(c)}(\zeta) \left(\frac{\partial \psi_f}{\partial y} + \frac{\partial \varphi_f}{\partial x} \right) \right] \\ \gamma_{xz}^{(c)}(x, y, \zeta) &= \frac{df_d^{(c)}}{d\zeta} \psi_f(x, y) \quad \gamma_{yz}^{(c)}(x, y, \zeta) = \frac{df_d^{(c)}}{d\zeta} \varphi_f(x, y) \end{aligned} \quad (2.9)$$

— the lower face ($\chi_c/2 \leq \zeta \leq 1/2$)

$$\begin{aligned} \varepsilon_x^{(lf)}(x, y, \zeta) &= -h \left[\zeta \frac{\partial^2 w}{\partial x^2} - f_d^{(lf)}(\zeta) \frac{\partial \psi_f}{\partial x} \right] \\ \varepsilon_y^{(lf)}(x, y, \zeta) &= -h \left[\zeta \frac{\partial^2 w}{\partial y^2} - f_d^{(lf)}(\zeta) \frac{\partial \varphi_f}{\partial y} \right] \\ \gamma_{xy}^{(lf)}(x, y, \zeta) &= -h \left[2\zeta \frac{\partial^2 w}{\partial x \partial y} - f_d^{(lf)}(\zeta) \left(\frac{\partial \psi_f}{\partial y} + \frac{\partial \varphi_f}{\partial x} \right) \right] \\ \gamma_{xz}^{(lf)}(x, y, \zeta) &= \frac{df_d^{(lf)}}{d\zeta} \psi_f(x, y) \quad \gamma_{yz}^{(lf)}(x, y, \zeta) = \frac{df_d^{(lf)}}{d\zeta} \varphi_f(x, y) \end{aligned} \quad (2.10)$$

Consequently, the stresses are derived:

— the upper face ($-1/2 \leq \zeta \leq -\chi_c/2$)

$$\begin{aligned} \sigma_x^{(uf)}(x, y, \zeta) &= \frac{E_f}{1 - \nu^2} [\varepsilon_x^{(uf)}(x, y, \zeta) + \nu \varepsilon_y^{(uf)}(x, y, \zeta)] \\ \sigma_y^{(uf)}(x, y, \zeta) &= \frac{E_f}{1 - \nu^2} [\varepsilon_y^{(uf)}(x, y, \zeta) + \nu \varepsilon_x^{(uf)}(x, y, \zeta)] \\ \tau_{xy}^{(uf)}(x, y, \zeta) &= \frac{E_f}{2(1 + \nu)} \gamma_{xy}^{(uf)}(x, y, \zeta) \quad \tau_{xz}^{(uf)}(x, y, \zeta) = \frac{E_f}{2(1 + \nu)} \gamma_{xz}^{(uf)}(x, y, \zeta) \\ \tau_{yz}^{(uf)}(x, y, \zeta) &= \frac{E_f}{2(1 + \nu)} \gamma_{yz}^{(uf)}(x, y, \zeta) \end{aligned} \quad (2.11)$$

— the core ($-\chi_c/2 \leq \zeta \leq \chi_c/2$)

$$\begin{aligned}
 \sigma_x^{(c)}(x, y, \zeta) &= \frac{E_f}{1-\nu^2} [\varepsilon_x^{(c)}(x, y, \zeta) + \nu \varepsilon_y^{(c)}(x, y, \zeta)] f_c(\zeta) \\
 \sigma_y^{(c)}(x, y, \zeta) &= \frac{E_f}{1-\nu^2} [\varepsilon_y^{(c)}(x, y, \zeta) + \nu \varepsilon_x^{(c)}(x, y, \zeta)] f_c(\zeta) \\
 \tau_{xy}^{(c)}(x, y, \zeta) &= \frac{E_f}{2(1+\nu)} \gamma_{xy}^{(c)}(x, y, \zeta) f_c(\zeta) \\
 \tau_{xz}^{(c)}(x, y, \zeta) &= \frac{E_f}{2(1+\nu)} \gamma_{xz}^{(c)}(x, y, \zeta) f_c(\zeta) \\
 \tau_{yz}^{(c)}(x, y, \zeta) &= \frac{E_f}{2(1+\nu)} \gamma_{yz}^{(c)}(x, y, \zeta) f_c(\zeta)
 \end{aligned} \tag{2.12}$$

— the lower face ($\chi_c/2 \leq \zeta \leq 1/2$)

$$\begin{aligned}
 \sigma_x^{(lf)}(x, y, \zeta) &= \frac{E_f}{1-\nu^2} [\varepsilon_x^{(lf)}(x, y, \zeta) + \nu \varepsilon_y^{(lf)}(x, y, \zeta)] \\
 \sigma_y^{(lf)}(x, y, \zeta) &= \frac{E_f}{1-\nu^2} [\varepsilon_y^{(lf)}(x, y, \zeta) + \nu \varepsilon_x^{(lf)}(x, y, \zeta)] \\
 \tau_{xy}^{(lf)}(x, y, \zeta) &= \frac{E_f}{2(1+\nu)} \gamma_{xy}^{(lf)}(x, y, \zeta) & \tau_{xz}^{(lf)}(x, y, \zeta) &= \frac{E_f}{2(1+\nu)} \gamma_{xz}^{(lf)}(x, y, \zeta) \\
 \tau_{yz}^{(lf)}(x, y, \zeta) &= \frac{E_f}{2(1+\nu)} \gamma_{yz}^{(lf)}(x, y, \zeta)
 \end{aligned} \tag{2.13}$$

where Poisson's ν ratio is constant for this plate.

3. The analytical study of the elastic buckling of the plate

The elastic strain energy of the plate

$$U_{\varepsilon, \gamma} = \frac{E_f h}{2(1-\nu^2)} \int_0^a \int_0^b [\Phi_{\varepsilon, \gamma}^{(uf)}(x, y) + \Phi_{\varepsilon, \gamma}^{(c)}(x, y) + \Phi_{\varepsilon, \gamma}^{(lf)}(x, y)] dx dy \tag{3.1}$$

where

$$\begin{aligned}
 \Phi_{\varepsilon, \gamma}^{(uf)}(x, y) &= \Phi_{\varepsilon}^{(uf)}(x, y) + \Phi_{\gamma}^{(uf)}(x, y) \\
 \Phi_{\varepsilon}^{(uf)}(x, y) &= \int_{-1/2}^{-\chi_c/2} \left\{ [\varepsilon_x^{(uf)}(x, y, \zeta)]^2 + 2\nu \varepsilon_x^{(uf)}(x, y, \zeta) \varepsilon_y^{(uf)}(x, y, \zeta) + [\varepsilon_y^{(uf)}(x, y, \zeta)]^2 \right\} d\zeta \\
 \Phi_{\gamma}^{(uf)}(x, y) &= \frac{1-\nu}{2} \int_{-1/2}^{-\chi_c/2} \left\{ [\gamma_{xy}^{(uf)}(x, y, \zeta)]^2 + [\gamma_{xz}^{(uf)}(x, y, \zeta)]^2 + [\gamma_{yz}^{(uf)}(x, y, \zeta)]^2 \right\} d\zeta \\
 \Phi_{\varepsilon, \gamma}^{(c)}(x, y) &= \Phi_{\varepsilon}^{(c)}(x, y) + \Phi_{\gamma}^{(c)}(x, y) & \Phi_{\varepsilon, \gamma}^{(lf)}(x, y) &= \Phi_{\varepsilon}^{(lf)}(x, y) + \Phi_{\gamma}^{(lf)}(x, y) \\
 \Phi_{\varepsilon}^{(c)}(x, y) &= \int_{-1/2}^{-\chi_c/2} \left\{ [\varepsilon_x^{(c)}(x, y, \zeta)]^2 + 2\nu \varepsilon_x^{(c)}(x, y, \zeta) \varepsilon_y^{(c)}(x, y, \zeta) + [\varepsilon_y^{(c)}(x, y, \zeta)]^2 \right\} f_c(\zeta) d\zeta
 \end{aligned}$$

$$\begin{aligned}\Phi_\gamma^{(c)}(x, y) &= \frac{1-\nu}{2} \int_{-1/2}^{-\chi_c/2} \left\{ [\gamma_{xy}^{(c)}(x, y, \zeta)]^2 + [\gamma_{xz}^{(c)}(x, y, \zeta)]^2 + [\gamma_{yz}^{(c)}(x, y, \zeta)]^2 \right\} f_c(\zeta) d\zeta \\ \Phi_\varepsilon^{(lf)}(x, y) &= \int_{-1/2}^{-\chi_c/2} \left\{ [\varepsilon_x^{(lf)}(x, y, \zeta)]^2 + 2\nu\varepsilon_x^{(lf)}(x, y, \zeta)\varepsilon_y^{(lf)}(x, y, \zeta) + [\varepsilon_y^{(lf)}(x, y, \zeta)]^2 \right\} d\zeta \\ \Phi_\gamma^{(lf)}(x, y) &= \frac{1-\nu}{2} \int_{-1/2}^{-\chi_c/2} \left\{ [\gamma_{xy}^{(lf)}(x, y, \zeta)]^2 + [\gamma_{xz}^{(lf)}(x, y, \zeta)]^2 + [\gamma_{yz}^{(lf)}(x, y, \zeta)]^2 \right\} d\zeta\end{aligned}$$

The work of the load is

$$W = \frac{1}{2} \int_0^a \int_0^b \left[N_x \left(\frac{\partial w}{\partial x} \right)^2 + N_y \left(\frac{\partial w}{\partial y} \right)^2 \right] dx dy \quad (3.2)$$

Based on the principle of stationary total potential energy $\delta(U_{\varepsilon, \gamma} - W) = 0$ with consideration of the expressions in Eqs. (3.1) and (3.2), after integration and simple transformation, three differential equations of equilibrium of this rectangular sandwich plate are obtained in the following form

$$\begin{aligned}D_o \left\{ C_{ww} \nabla^4 w(x, y) - C_{w\theta} \left[\frac{\partial}{\partial x} \nabla^2 \psi_f(x, y) + \frac{\partial}{\partial y} \nabla^2 \varphi_f(x, y) \right] \right\} + N_x \frac{\partial^2 w}{\partial x^2} + N_y \frac{\partial^2 w}{\partial y^2} &= 0 \\ C_{w\theta} \frac{\partial}{\partial x} \nabla^2 w(x, y) - C_{\theta\theta} \left[\frac{\partial^2 \psi_f}{\partial x^2} + \frac{1-\nu}{2} \frac{\partial^2 \psi_f}{\partial y^2} + \frac{1+\nu}{2} \frac{\partial^2 \varphi_f}{\partial x \partial y} \right] + C_\theta \frac{\psi_f(x, y)}{h^2} &= 0 \\ C_{w\theta} \frac{\partial}{\partial y} \nabla^2 w(x, y) - C_{\theta\theta} \left[\frac{1+\nu}{2} \frac{\partial^2 \psi_f}{\partial x \partial y} + \frac{1-\nu}{2} \frac{\partial^2 \varphi_f}{\partial x^2} + \frac{\partial^2 \varphi_f}{\partial y^2} \right] + C_\theta \frac{\varphi_f(x, y)}{h^2} &= 0\end{aligned} \quad (3.3)$$

where the dimensionless coefficients are

$$\begin{aligned}C_{ww} &= 1 - \chi_c^3 + 12 \int_{-\chi_c/2}^{\chi_c/2} \zeta^2 f_c(\zeta) d\zeta \\ C_{\theta\theta} &= 12 \left(2 \int_{-\chi_c/2}^{1/2} [f_d^{(lf)}(\zeta)]^2 d\zeta + \int_{-\chi_c/2}^{\chi_c/2} [f_d^{(c)}(\zeta)]^2 f_c(\zeta) d\zeta \right) \\ C_{w\theta} &= 3(1 - \chi_c^2) C_f + \frac{1}{40} (4 - 5\chi_c^3 + \chi_c^5) + 12 \int_{-\chi_c/2}^{\chi_c/2} \zeta f_d^{(c)}(\zeta) f_c(\zeta) d\zeta \\ C_\theta &= \frac{1-\nu}{2} \left(\frac{1}{80} (8 - 15\chi_c + 10\chi_c^3 - 3\chi_c^5) + 12 \int_{-\chi_c/2}^{\chi_c/2} \frac{[\overline{Q}_z^{(c)}(\zeta)]^2}{f_c(\zeta)} d\zeta \right)\end{aligned}$$

and

$$D_o = \frac{E_f h^3}{12(1-\nu^2)} \text{ [Nmm]}$$

Taking into account the papers by Magnucki *et al.* (2019) as well as Magnucki and Magnucka-Blandzi (2021), two unknown dimensionless displacement functions of the faces are assumed as follows

$$\psi_f(x, y) = \frac{\partial \theta}{\partial x} \quad \varphi_f(x, y) = \frac{\partial \theta}{\partial y} \quad (3.4)$$

where $\theta(x, y)$ [mm] is the generalised displacement. Thus, the three differential equations of equilibrium convert into the following two equations

$$\begin{aligned} D_o[C_{ww}\nabla^4 w(x, y) - C_{w\theta}\nabla^4 \theta(x, y)] + N_x \frac{\partial^2 w}{\partial x^2} + N_y \frac{\partial^2 w}{\partial y^2} &= 0 \\ C_{w\theta}\nabla^2 w(x, y) - C_{\theta\theta}\nabla^2 \theta(x, y) + C_\theta \frac{\theta(x, y)}{h^2} &= 0 \end{aligned} \quad (3.5)$$

These equations are approximately solved, and so two typical unknown functions describing the shape of the deformed structure are assumed in a general form as follows

$$w(x, y) = w_a \sin\left(m\pi \frac{x}{a}\right) \sin\left(n\pi \frac{y}{b}\right) \quad \theta(x, y) = \theta_a \sin\left(m\pi \frac{x}{a}\right) \sin\left(n\pi \frac{y}{b}\right) \quad (3.6)$$

where: w_a [mm], θ_a [mm] – coefficients of these functions, m, n – natural numbers.

Substituting these functions into Eqs. (3.5), after simple transformations, one obtains

$$\theta_a = \frac{C_{w\theta}}{C_{\theta\theta} + \frac{ab}{\pi^2 h^2 a_{mn}}} w_a \quad m^2 \frac{b}{a} N_x + n^2 \frac{a}{b} N_y = \frac{\pi^2}{ab} (1 - C_{se}) \alpha_{mn}^2 D_p \quad (3.7)$$

where the dimensionless coefficient is expressed as

$$\alpha_{mn} = m^2 \frac{b}{a} + n^2 \frac{a}{b}$$

and $D_p = C_{ww} C_o$ [Nmm] is the flexural rigidity of this plate, while the coefficient of the shear effect is

$$C_{se} = \frac{\pi^2 \alpha_{mn}}{\pi^2 \alpha_{mn} C_{\theta\theta} + \frac{ab}{h^2} C_\theta} \frac{C_{w\theta}^2}{C_{ww}} \quad (3.8)$$

Moreover, for further study, the plate load is assumed in the following form

$$N_x = c_x N_o \quad N_y = c_y N_o \quad (3.9)$$

where: c_x and c_y are positive dimensionless coefficients. Thus, the critical load is as follows

$$N_{0,CR} = \min_{m,n} \left[(1 - C_{se}) \frac{\alpha_{mn}^2}{\alpha_N} \right] \frac{\pi^2 D_p}{ab} \quad (3.10)$$

where another dimensionless coefficient is introduced

$$\alpha_N = m^2 \frac{b}{a} c_x + n^2 \frac{a}{b} c_y$$

Consequently, the critical load of the square plate ($b = a, m = n = 1, \alpha_{mn} = 2$) is in the form

$$N_{0,CR} = 4\pi^2 \frac{1 - C_{se}}{c_x + c_y} \frac{D_p}{a^2} \quad (3.11)$$

For the particular case of the homogeneous square plate without the shear effect ($C_{ww} = 1, D_p = C_o, C_{se} = 0, c_x = 1, c_y = 0$), one obtains the classical critical stress

$$\sigma_{x,CR} = \frac{\pi^2}{3(1 - \nu^2)} E \left(\frac{h}{a} \right)^2 \quad (3.12)$$

Exemplary calculations are carried out for square sandwich plates with the selected following data: $E_f = 72000$ MPa, $a = b = 2000$ mm, $h = 30$ mm, $h_f = 1.5$ mm, $h_c = 27$ mm, $\chi_c = 9/10$,

Table 1. The results of analytical calculations for $n_e = 2$

k	0	0.5	$1 - e_c$
C_{se}	0.00637523	0.00716652	0.0102967
$N_{0,CR}^{(lc-1)}$ [N/mm]	1081.99	1074.65	1065.34
$N_{0,CR}^{(lc-2)}$ [N/mm]	721.33	716.43	710.26
$N_{0,CR}^{(lc-3)}$ [N/mm]	541.00	537.32	532.67

Table 2. The results of analytical calculations for $n_e = 10$

k	0	0.5	$1 - e_c$
C_{se}	0.00860048	0.00878646	0.00961103
$N_{0,CR}^{(lc-1)}$ [N/mm]	813.91	813.15	811.92
$N_{0,CR}^{(lc-2)}$ [N/mm]	542.61	542.10	541.28
$N_{0,CR}^{(lc-3)}$ [N/mm]	406.96	406.58	405.96

$e_c = 1/24$, $\nu = 0.3$, $k = (0, 0.5, 1 - e_c)$ and for three load cases: $lc - 1$ ($c_x = 1.0$, $c_y = 0$), $lc - 2$ ($c_x = 1.0$, $c_y = 0.5$), $lc - 3$ ($c_x = 1.0$, $c_y = 1.0$). The assumed parameters are exemplary, however, the mechanical properties of the faces are typical for aluminium alloys, while the core can be considered to be a densely graded aluminium foam. The results of the analytical calculations of the shear coefficient C_{se} (3.8) and critical load values $N_{0,CR}^{(lc-i)}$ (3.11) for three load cases ($lc - i$, $i = 1, 2, 3$) and for two values of the exponent-natural number $n_e = 2, 10$ are specified in Tables 1 and 2.

Analysing the results of the above calculations, it can be noted that an increase in the stiffness near the neutral plane has negligible influence on the critical load. Such an observation is consistent with the literature provided. This confirms that five-layer plates with symmetrically varying mechanical properties are insignificantly more resistant to buckling than three-layer structures. Assuming that Young's modulus is connected with density of the material, the three-layer plates can be characterised by a smaller mass while maintaining the same buckling load. As expected, an increase of n_e leads to a decrease in the critical load, since this parameter refers to the transition rate of Young's modulus (Fig. 1) between the faces and the core of the plate. The faster Young's modulus of the face reaches the value of e_c in the core, the smaller the overall stiffness of the plate, thus one may notice a decrease in buckling performance.

4. The numerical FEM study of the elastic buckling of the plate

To provide more insight into the study, numerical finite element method (FEM) analyses are carried out in Ansys 2021 R2 system. The problem is solved using linear static structural analysis. The parameters describing geometry as well as the material are consistent with the analytical study.

Typically, the buckling behaviour of a structure should be studied without symmetry boundary conditions since one cannot predict whether the first buckling mode is symmetric. As an accurate representation of Young's modulus distribution (Fig. 2) requires a relatively large number of finite elements across the thickness, this problem becomes computationally demanding. To address this issue, preliminary analyses with a reduced number of elements are performed using the full plate model. Those confirm that the first buckling mode is symmetric just like in the case of homogeneous square plates, and thus a quarter of the plate can be considered in the numerical analysis.

The geometry of the quarter thin-walled plate is shown in Fig. 4. The applied boundary conditions assume simply supported edges and symmetry boundary conditions in the faces coincident with symmetry planes. The first of them is introduced by restraining translations w towards z axis on two edges highlighted in blue in Fig. 4. The symmetric behaviour is included by blocking the translations u and v , i.e. towards x and y axes. These components refer to normal directions to the faces highlighted in green in Fig. 4. The compressive loads N_x and N_y acting on the faces are shown in red in Fig. 4. Following the introduced loads and boundary conditions, those are consistent with the analytical study.

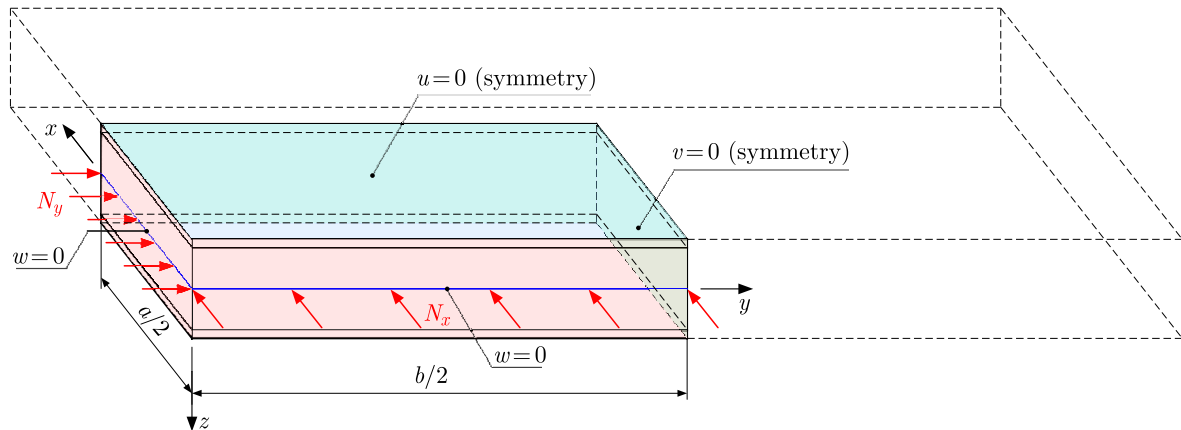


Fig. 4. The geometry of a quarter of the plate and the applied boundary conditions

The geometry of the structure is divided into first-order hexahedral finite elements SOLID185. The value of Young's modulus from Fig. 2 is mapped to the centres of finite elements. The choice of the first order elements provides a more detailed Young's modulus distribution (Fig. 2) than second-order elements for the same number of nodes. The resulting finite element model is shown in Fig. 5, where Fig. 5a shows the model with the reduced number of finite elements for better readability, while Fig. 5b refers to the actual mesh. The latter is the result of a mesh convergence study and consists of 48 elements across the thickness and 91 elements along the sides of the square plate. The total number of nodes and elements is 414736 and 397488, respectively. The aspect ratio of the elements is approximately 18. It has been found that a further increase in the aspect ratio can cause the inability to achieve the convergence of results. In addition, a numerical analysis is performed for a homogeneous plate with consistent parameters applied in the analytical study. Using the well-known expression for the critical stress described in the literature (Eq. (3.12)) for comparison, the relative difference between the results is 1.38%, showing an adequate numerical modelling.

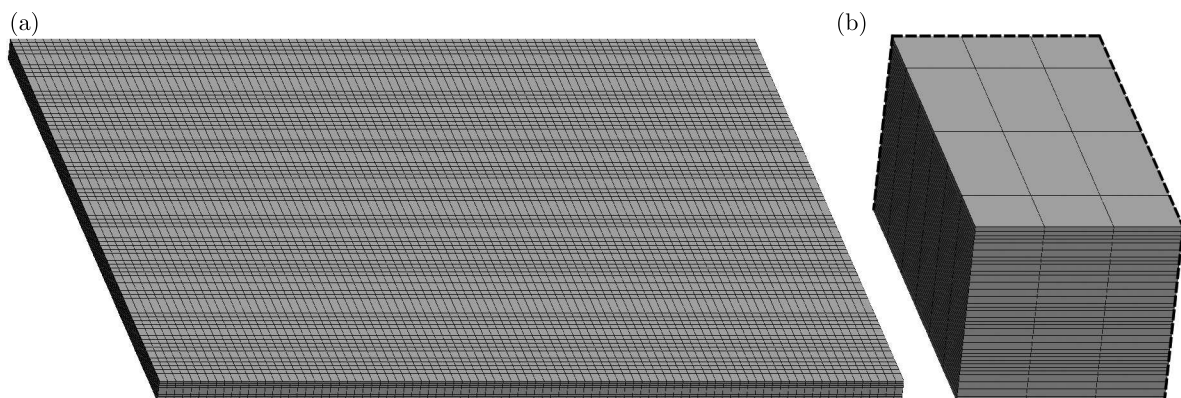


Fig. 5. Model divided into finite elements

Following Young's modulus function in Eqs. (2.2), (2.3) shown in Fig. 2, its distribution depends on the parameters k and n_e . The first of them refers to the relationship between Young's modulus on the external faces and the middle of the plate. The latter describes the pace of its transition. Exemplary Young's modulus distributions are shown in Fig. 6 for two sets of parameters. The effect of non-uniform mechanical property in Ansys software is achieved by linking the so-called "field variable" to the elastic properties of the material. This variable can be described by an external text file, which in this case consists of numerous coordinates in a three-dimensional coordinate system within the plate volume and consistent values of Young's modulus in a dimensionless form. The software interpolates the values provided to calculate Young's modulus in the centre of each finite element. The more points are provided in the text file, the more accurate the representation of the selected mechanical parameter becomes.

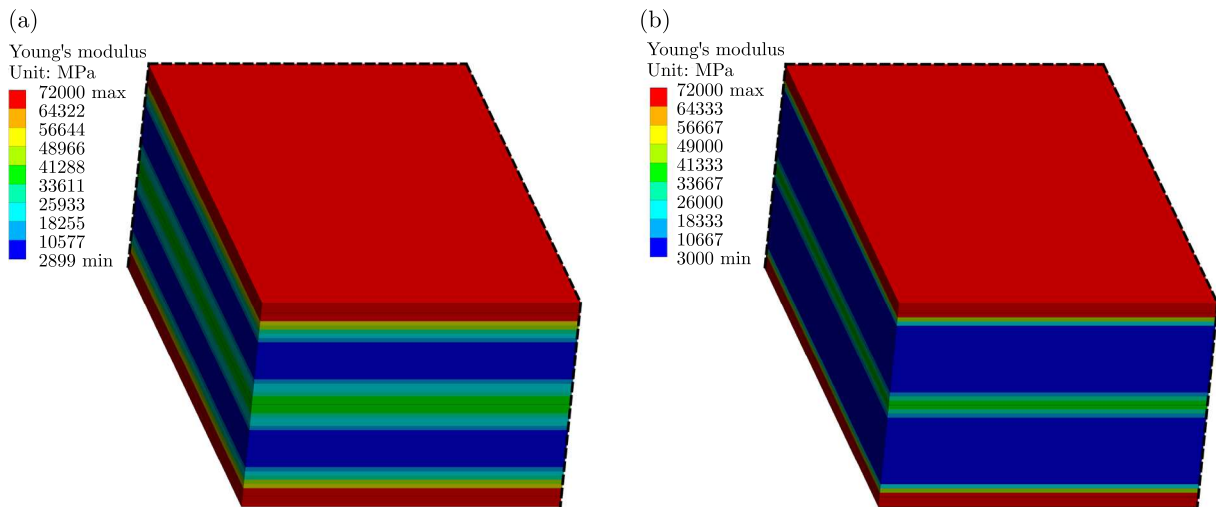


Fig. 6. Exemplary Young's modulus distribution for different material parameters

As expected, the first buckling mode (Fig. 7) is similar to the case of homogeneous and sandwich plates. Despite the fact that its symmetry is enforced by the applied boundary conditions, such behaviour was confirmed in the FEM study for the model with its complete geometry considered.

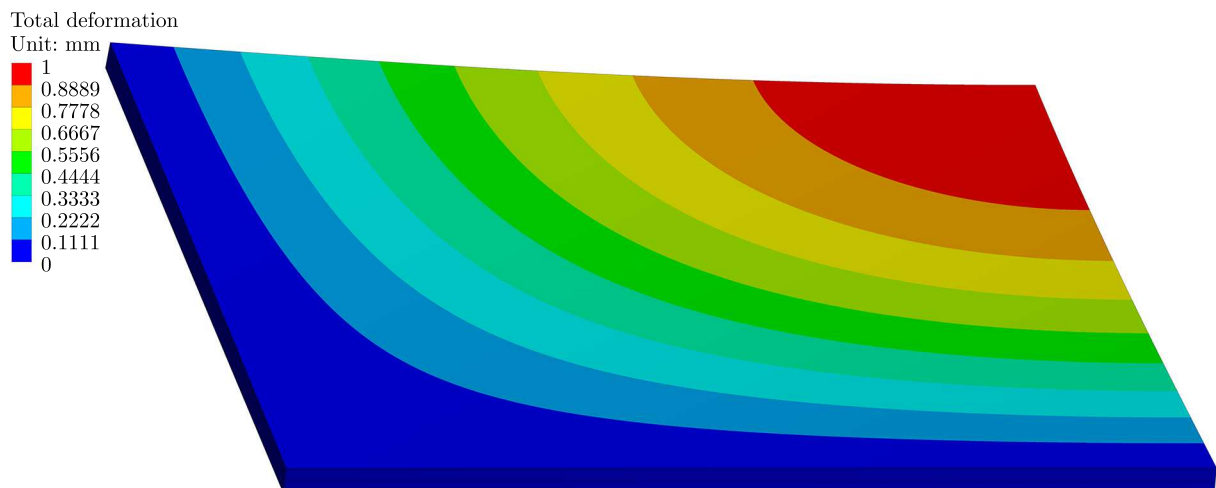


Fig. 7. First buckling mode for $k = 0.5$, $n_e = 10$

To provide more insight into the results, they are summarised in Tables 3 and 5 for $n_e = 2$ and $n_e = 10$, respectively. These are compared to the analytical solution by calculating the

relative difference shown in Tables 4 and 6, while the analytical solution is referred to as the reference value.

Table 3. Results of numerical FEM calculations for $n_e = 2$

k	0	0.5	$1 - e_c$
$N_{0,CR}^{(lc-1)}$ [N/mm]	1051.62	1042.21	1027.89
$N_{0,CR}^{(lc-2)}$ [N/mm]	701.11	694.87	685.39
$N_{0,CR}^{(lc-3)}$ [N/mm]	525.83	521.15	514.05

Table 4. Relative differences in analytical and numerical FEM calculations for $n_e = 2$

k	0	0.5	$1 - e_c$
$\delta N_{0,CR}^{(lc-1)}$ [%]	2.89	3.11	3.64
$\delta N_{0,CR}^{(lc-2)}$ [%]	2.88	3.10	3.63
$\delta N_{0,CR}^{(lc-3)}$ [%]	2.88	3.10	3.62

Table 5. Results of numerical FEM calculations for $n_e = 10$

k	0	0.5	$1 - e_c$
$N_{0,CR}^{(lc-1)}$ [N/mm]	786.60	785.63	783.26
$N_{0,CR}^{(lc-2)}$ [N/mm]	524.44	523.80	522.24
$N_{0,CR}^{(lc-3)}$ [N/mm]	393.33	392.85	391.68

Table 6. Relative differences in analytical and numerical FEM calculations for $n_e = 10$

k	0	0.5	$1 - e_c$
$\delta N_{0,CR}^{(lc-1)}$ [%]	3.47	3.50	3.66
$\delta N_{0,CR}^{(lc-2)}$ [%]	3.46	3.49	3.65
$\delta N_{0,CR}^{(lc-3)}$ [%]	3.47	3.49	3.65

5. Conclusions

The advancement in manufacturing methods allows for the designing of structures characterised by variable mechanical parameters in a controlled manner. This property can be used to achieve more efficient structural behaviour of load-carrying members. The proposed symmetric variation in Young's modulus allows the description of different structures, including homogeneous structures, three-layer and five-layer structures, with a smooth and controlled transition rate between layers.

Many studies in the field of composites refer to numerous shear deformation theories that are based on general predefined shear deformation functions that are usually suitable for specific FGMs. To solve the problem given in the presented paper, a novel nonlinear shear deformation theory of a straight normal line was applied. Unlike other theories, the derivation of the shear deformation function can be achieved analytically without assuming its form in advance; thus, it allows the study of FGMs and sandwich structures with various properties.

The influence of the studied parameters that affect Young's modulus distributions can be considered to be predictable. Both analyses have shown that an increase in Young's modulus transition rate from the faces to the core results in a reduced value of the critical load, as the overall stiffness of this structure is lower. Similarly, an increase of Young's modulus in the

neutral plane area of the plate has quite a limited effect on buckling resistance. Considering the consistency of the results in analytical and numerical applications, one may notice that there is a limited relationship between Young's modulus distribution and the results in both methods.

In general, the numerical study shows good agreement with the analytical results, where the maximum relative difference in critical loads reaches 3.7%. Having in mind the approximate nature of the obtained solution and numerical errors, such a difference can be considered satisfactory.

Acknowledgement

The paper is developed based on the scientific activity of the Łukasiewicz Research Network – Poznan Institute of Technology, Rail Vehicles Center, and the statutory activity of the Institute of Mathematics and Institute of Applied Mechanics, Poznan University of Technology, funded by the Ministry of Science and Higher Education in Poland (grant No. 0612/SBAD/3605).

References

1. ADHIKARI B., DASH P., SINGH B.N., 2020, Buckling analysis of porous FGM sandwich plates under various types nonuniform edge compression based on higher order shear deformation theory, *Composite Structures*, **251**, 112597
2. AGUIB S., CHIKH N., KOBZILI L., DJEDID T., NOUR A., MELOUSSI M., 2021, Analysis of buckling stability behavior of hybrid plate using Ritz approach and numerical simulation, *Structures*, **34**, 3222-3237.
3. BERDICHEVSKY V.L., 2010, An asymptotic theory of sandwich plates, *International Journal of Engineering Science*, **48**, 3, 383-404
4. BIRMAN V., KARDOMATEAS G.A., 2018, Review of current trends in research and applications of sandwich structures, *Composites Part B: Engineering*, **142**, 221-240
5. BOUAZZA M., BECHERI T., BOUCHETA A., BENSEDDIQ N., 2019, Bending behavior of laminated composite plates using the refined four-variable theory and the finite element method, *Earthquakes and Structures*, **17**, 3, 257-270
6. BOUAZZA M., BENSEDDIQ N., 2015, Analytical modeling for the thermoelastic buckling behavior of functionally graded rectangular plates using hyperbolic shear deformation theory under thermal loadings, *Multidiscipline Modeling in Materials and Structures*, **11**, 4, 558-578
7. BOUAZZA M., HAMMADI F., KHADIR M., 2010, Bending analysis of symmetrically laminated plates, *Leonardo Journal of Sciences*, **16**, 105-116
8. CARRERA E., BRISCHETTO S., 2009, A survey with numerical assessment of classical and refined theories for the analysis of sandwich plates, *Applied Mechanics Review*, **62**, 1, 010803
9. DHURIA M., GROVER N., GOYAL K., 2021, Influence of porosity distribution on static and buckling responses of porous functionally graded plates, *Structures*, **34**, 1458-1474
10. ELLALI M., AMARA K., BOUAZZA M., BOURADA F., 2015, The buckling of piezoelectric plates on Pasternak elastic foundation using higher-order shear deformation plate theories, *Smart Structures and Systems*, **21**, 1, 113-122
11. FOROUTAN K., CARRERA E., PAGANI A., AHMADI H., 2021, Post-buckling and large-deflection analysis of a sandwich FG plate with FG porous core using Carrera's Unified Formulation, *Composite Structures*, **272**, 114189
12. GROVER N., MAITI D.K., SINGH B.N., 2013, A new inverse hyperbolic shear deformation theory for static and buckling analysis of laminated composite and sandwich plates, *Composite Structures*, **95**, 667-675

13. KATILI I., BATOZ J.-L., BOUABDALLAH S., MAKNUN I.J., KATILI A.M., 2023, Discrete shear projection method for mechanical buckling analysis of FGM sandwich plates, *Composite Structures*, **312**, 116825
14. KOŁAKOWSKI Z., MANIA R.J., 2015, Dynamic response of thin FG plates with a static unsymmetrical stable postbuckling path, *Thin-Walled Structures*, **86**, 10-17
15. LOPATIN A.V., MOROZOV E.V., 2013, Buckling of a uniformly compressed rectangular SSCF composite sandwich plate, *Composite Structures*, **105**, 108-115
16. MAGNUCKA-BLANDZI E., MAGNUCKI K., STAWECKI W., 2021, Bending and buckling of a circular plate with symmetrically varying mechanical properties, *Applied Mathematical Modelling*, **89**, 2, 1198-1205
17. MAGNUCKI K., 2022, An individual shear deformation theory of beams with consideration of the Zhuravsky shear stress formula, *Current Perspectives and New Directions in Mechanics, Modelling and Design of Structural Systems*, 682-689
18. MAGNUCKI K., MAGNUCKA-BLANDZI E., 2021, Generalization of a sandwich structure model: Analytical studies of bending and buckling problems of rectangular plates, *Composite Structures*, **255**, 112944.
19. MAGNUCKI K., MAGNUCKA-BLANDZI E., WITTENBECK L., 2023, Elastic buckling of a generalized cylindrical sandwich panel under axial compression, *Bulletin of the Polish Academy of Sciences – Technical Sciences*, **71**, 2, 144623
20. MAGNUCKI K., WITKOWSKI D., MAGNUCKA-BLANDZI E., 2019, Buckling and free vibrations of rectangular plates with symmetrically varying mechanical properties – analytical and FEM studies, *Composite Structures*, **220**, 355-361
21. MANTARI J.L., MONGE J.C., 2016, Buckling, free vibration and bending analysis of functionally graded sandwich plates based on an optimized hyperbolic unified formulation, *International Journal of Mechanical Sciences*, **119**, 170-186
22. MANTARI J.L., OKTEM A.S., SOARES C.G., 2012, A new higher order shear deformation theory for sandwich and composite laminated plates, *Composites Part B: Engineering*, **43**, 3, 1489-1499
23. MARCZAK J., JĘDRYSIAK J., 2015, Tolerance modelling of vibrations of periodic three-layered plates with inert core, *Composite Structures*, **134**, 854-861
24. MEICHE N.E., TOUNSI A., ZIANE N., MECHAB I., ADDA BEDIA E.A., 2011, A new hyperbolic shear deformation theory for buckling and vibration of functionally graded sandwich plate, *International Journal of Mechanical Sciences*, **53**, 4, 237-247
25. SAHOO R., SINGH B.N., 2013, A new shear deformation theory for the static analysis of laminated composite and sandwich plates, *International Journal of Mechanical Sciences*, **75**, 324-336
26. SAHOO R., SINGH B.N., 2014, A new trigonometric zigzag theory for buckling and vibration analysis of laminated composite and sandwich plates, *Composite Structures*, **117**, 316-332
27. SITLI Y., MHADA K., BOURIHANE O., RHANIM H., 2021, Buckling and post-buckling analysis of a functionally graded material (FGM) plate by the Asymptotic Numerical Method, *Structures*, **31**, 1031-1040
28. SOBHY M., 2016, An accurate shear deformation theory for vibration and buckling of FGM sandwich plates in hygrothermal environment, *International Journal of Mechanical Sciences*, **110**, 62-77
29. YANG M., QIAO P., 2005, Higher-order impact modeling of sandwich structures with flexible core, *International Journal of Solids and Structures*, **42**, 20, 5460-5490